AIP | Journal of Applied Physics

Temperature dependent carrier dynamics in telecommunication band InAs quantum dots and dashes grown on InP substrates

Nahid A. Jahan, Claus Hermannstädter, Jae-Hoon Huh, Hirotaka Sasakura, Thomas J. Rotter et al.

Citation: J. Appl. Phys. **113**, 033506 (2013); doi: 10.1063/1.4775768
View online: http://dx.doi.org/10.1063/1.4775768
View Table of Contents: http://jap.aip.org/resource/1/JAPIAU/v113/i3
Published by the American Institute of Physics.

JOURNAL OF APPLIED PHYSICS **113**, 033506 (2013)

Temperature dependent carrier dynamics in telecommunication band InAs quantum dots and dashes grown on InP substrates

Nahid A. Jahan,[1,2,a)] Claus Hermannstädter,[1] Jae-Hoon Huh,[1] Hirotaka Sasakura,[1] Thomas J. Rotter,[3] Pankaj Ahirwar,[3] Ganesh Balakrishnan,[3] Kouichi Akahane,[4] Masahide Sasaki,[4] Hidekazu Kumano,[1] and Ikuo Suemune[1]
[1]*Research Institute for Electronic Science, Hokkaido University, Sapporo 001-0021, Japan*
[2]*Graduate School of Information Science and Technology, Hokkaido University, Sapporo 060-0814, Japan*
[3]*Center for High Technology Materials, University of New Mexico, 1313 Goddard SE Albuquerque, New Mexico 87106, USA*
[4]*National Institute of Information and Communications Technology, Koganei, Tokyo 184-8795, Japan*

(Received 18 September 2012; accepted 21 December 2012; published online 16 January 2013)

InAs quantum dots (QDs) grown on InP substrates can be used as light emitters in the telecommunication bands. In this paper, we present optical characterization of high-density circular quantum dots (QDots) grown on InP(311)B substrates and elongated dots (QDashes) grown on InP(001) substrates. We study the charge carrier transfer and luminescence thermal quenching mechanisms of the QDots and QDashes by investigating the temperature dependence of their time-integrated and time-resolved photoluminescence properties. This results in two different contributions of the thermal activation energies. The larger activation energies are attributed to the carrier escape to the barrier layer and the wetting layer (WL) from QDots and QDashes, respectively. The smaller activation energies are found to be originated from inter-dot/dash carrier transfer via coupled excited states. The variation of the average oscillator strength associated with the carrier re-distribution is discussed. The relation of the two activation energies is also quantitatively studied with the measurements of excited-state and ground-state energy separations. Finally, we show an approach to isolate individual quantum dots or dashes in a suitable nanostructure. © *2013 American Institute of Physics*. [http://dx.doi.org/10.1063/1.4775768]

I. INTRODUCTION

Numerous applications of semiconductor quantum dots (QDs) have been reported throughout the past decades. They have been widely used as promising and favorable active media in semiconductor QD lasers[1–7] with ensembles of QDs of the highest possible densities and also as photo-detectors.[8] Microscopic spectroscopy studies of individual semiconductor QDs have shown that single QDs have excellent potential at the heart of single photon sources[9–11] and sources of entangled photon pairs[12–14] for high-speed quantum information and communication. With the focus on practical QD based quantum communication through silica based fiber-optical networks, the attention is drawn to the telecommunication bands, especially on the O band (0.912–0.984 eV; 1.360–1.260 μm) and the C band (0.792–0.810 eV; 1.565–1.530 μm). To date the main part of the work on single QDs has been reported for shorter wavelength emission up to about 1.33 μm.[15,16] This includes dots grown on GaAs substrates, e.g., up to 7% lattice mismatched In(Ga)As/GaAs (III-V) QDs (0.93–1.5 eV; 1330–800 nm) and CdSe/ZnS (II-VI) QDs (1.8–3.5 eV; 700–350 nm) as well as the group-III-Nitrides with their respective energies from 1 to 6 eV (1200–200 nm). Ganapathy *et al.*[17] demonstrated a long emission wavelength over 1.5 μm at room temperature from InAs QDs grown on GaAs buried under increased nitrogen (N) content GaNAs strain-compensating layers. Lately, Semenova *et al.* reported 1.55 μm QD emission from InAs QDs grown by a demanding sophisticated method on GaAs substrate using metamorphic buffer layers.[18] Afterward, Strauss *et al.* demonstrated InAs QDs capped by a low N content GaInAs(N) quantum well grown on GaAs substrates emitting at about 1.3 μm, with a possible extension of the emission up to 1.48 μm at low temperature by adding N to the QDs directly, using an optimized molecular beam epitaxy (MBE) technique.[19] However, further extension of the QD emission to 1.55 μm for self-assembled In(Ga)As dots grown on GaAs substrates appears very difficult and thus implies the consideration of heterostructures grown on different substrates. InAs/InP heterostructures exhibit a substantially smaller lattice mismatch of only about 3%, which renders the suitability to obtain near-infrared emission (0.953–0.799 eV; 1.3–1.55 μm) with less effort. This consequently hauled our interest towards the study of InAs QDs grown on InP substrates, which is presented in this paper.

Hereafter, we want to introduce the following abbreviations: "QDots" for almost cylindrically symmetric quantum dots grown on InP(311)B substrates, "QDashes" for elongated dots and dashes grown on InP(001) substrates and the conventionally used "QDs" for both QDots and/or QDashes, without distinguishing between them, in a context where the exact definition is not particularly important.

For InAs/InP heterostructures, the formation of QDashes can be observed especially when grown on InP(001) substrates,[20,21] whereas InAs/InP QDots of circular symmetry can be grown on higher index substrates such as InP(311)B.[22,23]

a)Electronic mail: nahid@es.hokudai.ac.jp.

Moreover, the growth of telecom band InAs QDs on InP tends to result in QD ensembles of rather high density ($\sim 10^{11}\,cm^{-2}$). This can provide the possibility of inter-dot tunnel coupling among neighboring QDs. To date a number of studies on charge carrier transfer[24,25] have been performed on InAs QDs grown on GaAs. In most of the studies, it is suggested that when the temperature is increased to a certain extent, the wetting layer (WL) acts as the transit channel to transfer carriers among QDs.[26,27] But for high dot density other carrier transit channel may also exist. Only few experimental studies have been reported on carrier tunneling mechanism in such high-density InAs QDs grown on InP substrates.[28] Another important process which limits the QD PL and eventually leads to its thermal quenching is the thermal escape of charge carriers to the embedding matrix, i.e., the barrier and/or WL. The energetic separation between QDs and WL can be very small, such as for the typical Stranski-Krastanov growth[29] of self-assembled QDs. Therefore, the QDs confinement energy is an essential quantity when the QDs are to be used as photon sources at higher temperatures and in various applications such as QD lasers. This is especially the case when the system's temperature is increased above the liquid Helium temperature of 4.2 K.

In order to achieve higher confinement energies, the inclusion of a variety of higher-bandgap barrier materials was suggested and reported.[30–33] For group-III-As/P heterostructures, which are treated in this work, the highest energy gaps can be realized by increasing the Al content of the barrier material, which is, among others, discussed in detail by Schulz *et al.*[33] Based on these materials and heterostructures, detailed understanding of the carrier dynamics including the carrier transfer and thermal quenching mechanism of QD luminescence become inevitable. Innumerous study of thermal escape modeling has been investigated theoretically and experimentally so far in several publications.[26,27,34–40] Some of them reported that exciton escape is responsible for the quenching of the QD luminescence at high temperatures.[27,38,39] Some suggested the correlated electron-hole pair escape mechanism[40] and free electron or hole escape mechanism. In spite of these studies, the present research stage especially on the telecom-band QD structures is not yet conclusive. Moreover it is known that growth of InAs/InP QDs tends to result in high QD densities and the interactions among the neighboring QDs are not negligible. The WLs usually associated with QDs are also deeply involved in the steady and dynamic optical properties. These issues make the QD dynamic optical properties more complex.

In this paper, we study steady-state and dynamic temperature-dependent luminescence properties of telecommunication-band InAs QDs grown on InP and try to clarify the luminescence quenching mechanism. We investigate InAs/$In_{0.53}Al_{0.22}Ga_{0.25}As$ QDots grown on InP(311)B substrates and InAs/$In_{0.52}Al_{0.48}As$ QDashes grown on InP(001) substrates. We will show the presence of two thermal activation energies in the photoluminescence (PL) quenching processes of both QDots and QDashes. The PL quenching mechanism related to the one of the two activation energies is shown to be related to the carrier escape to the barrier or WL. We also discuss the absence of the WL in the QDot samples grown on InP(311)B substrates. The PL quenching mechanism related to the other activation energy is attributed to the inter-dot charge carrier transfer and this transfer mechanism is discussed with the measurements of the energy separation between the QD excited states and ground states (GS).[39] We will show that this inter-dot charge transfer results in the increase of the observed lifetime for the elevated temperature. The related temperature variation of the QD average oscillator strength (OS) for the GS transitions is quantitatively discussed.

Single QDs at elevated temperatures, e.g., as sources for single photons,[41,42] are another hot topic in recent research. We therefore present an approach and provide first results that show the applicability of high-density QDs as basis for single dot or dash applications at about 1.55 μm.

II. SAMPLE PREPERATION OF THE QDs

A. QDots in $In_{0.53}Al_{0.22}Ga_{0.25}As$ barriers

The InAs QDots were grown by solid source MBE on a lattice-matched $In_{0.53}Al_{0.22}Ga_{0.25}As$ buffer on an n-type InP(311)B substrate, where a high dot density and homogeneity, as well as a good rotational dot-symmetry can be achieved.[43–45] The samples feature an optically active layer of QDots with a nominal thickness of four to six monolayers (MLs) of InAs which is embedded between 150 nm thick $In_{0.53}Al_{0.22}Ga_{0.25}As$ barrier layers (Fig. 1(a)). An identical QDot layer on top of the upper barrier layer was added for atomic force microscope (AFM) imaging of the samples.

The AFM image conveys that the shape of the 4 ML InAs QDots is slightly ellipsoidal with a very uniform spatial distribution (Fig. 1(b)); the areal dot density is around $1.1 \times 10^{11}\,cm^{-2}$, the average lateral diameters of the QDots are 29 nm along the [−233] direction and 23 nm in the [01-1] direction, and the average height of the uncapped open dots is ~3.4 nm. The average distance between the 4 ML QDots is calculated to be 4.3 nm from the average dot density and the lateral diameters. In case of 6 ML QDot sample (AFM image not shown), the estimated average areal dot density is $1.12 \times 10^{11}\,cm^{-2}$ with the average lateral diameters of 30 nm in the [−233] direction and 25 nm in the [01-1]. The average distance between the QDots is calculated to be around 2 nm. However, it is clear in Fig. 1(b) that some QDots are much

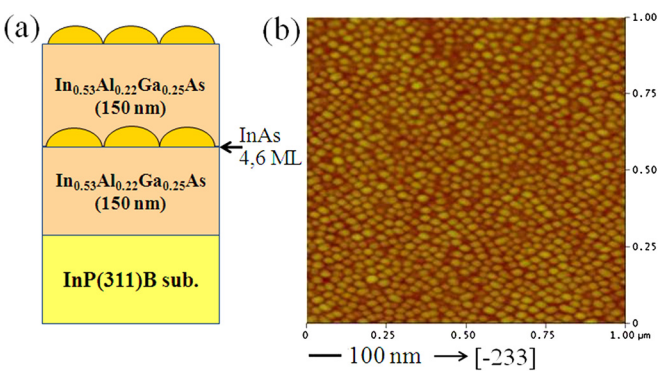

FIG. 1. (a) Schematic illustration of the InAs/$In_{0.53}Al_{0.22}Ga_{0.25}As$ QDot heterostructure. (b) $1 \times 1\,\mu m^2$ AFM image of the open dots on top of the 4 ML QDot sample.

closer to each other than others. This induces the coupling of the excited states between neighboring QDots as discussed later.

B. QDashes in $In_{0.52}Al_{0.48}As$ barriers

The QDash asymmetry, which depends on the relative surface migration along the [1-10] and [110] crystal directions, is influenced by both strain and surface bonds. Zinc-blende or tetrahedral structures create a bonding asymmetry on the (100) surface in two directions. Group-V stabilized surfaces show the tendency to form islands elongated along the [1-10] direction, while group-III stabilization leads to elongation along the [110] direction.[46,47] In the low strain growth mode, the directional property of the substrate is transferred to the islands grown on it. Moreover, the tendency of forming dash-like shapes was reported for InAs islands grown on InAlAs buffers on InP(001) substrates.[48]

In this work, the high density InAs QDash samples were grown by MBE on the lattice matched $In_{0.52}Al_{0.48}As$ buffer on InP(001) substrates. Besides lattice matching, another incentive of introducing the higher Aluminum content in the barrier layers is the increased confinement energy. The QDashes were grown by varying the nominal thickness of the optically active layer between three and six MLs of InAs (Fig. 2(a)). For these particular InAs/$In_{0.52}Al_{0.48}As$ QDash samples, we observed a less homogeneous distribution of InAs islands as compared to the aforementioned QDots. In some particular regions dashes are found very dense giving cluster like shape while in some regions they are separated. Both dash and elongated dot-like shapes can be also observed in the AFM image [see Fig. 2(b)]. The observed 6 ML QDashes appear favorably elongated along the [1-10] crystal direction with an aspect ratio of approximately 2.5:1 (60 and 24 nm average lateral diameters).

The average height of the uncapped QDashes is 1.9 nm and the overall areal density is about $5.1 \times 10^{10}\,cm^{-2}$. Although, the QDash samples show less-uniform distribution, by assuming a homogenous spatial distribution an average spacing of 5.8 nm between the neighboring 6 ML QDashes is estimated. Since some QDashes are much closer to each other, this also induces the coupling of the excited states between neighboring QDashes as discussed later.

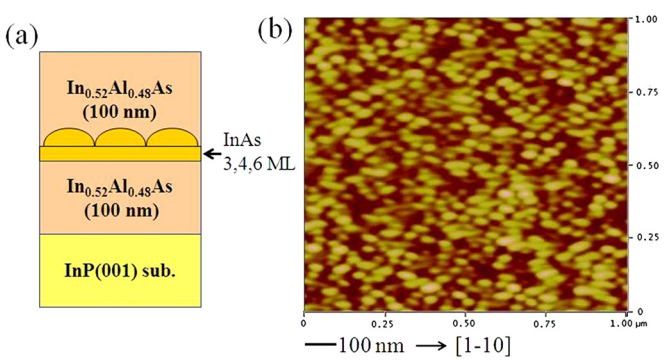

FIG. 2. (a) Schematic illustration of the InAs/$In_{0.52}Al_{0.48}As$ QDash heterostructure. (b) $1 \times 1\,\mu m^2$ AFM image of a 6 ML QDash sample without cap layer.

III. EXPERIMENTAL DETAILS

For PL spectroscopy of ensembles and individual QDs the samples were mounted in He-flow cryostats at temperatures between 4 and 300 K. High-energy lasers (above the energy of the InP substrate and $In_{0.53}Al_{0.22}Ga_{0.25}As$ barrier energy gap) were used for optical excitation, and different detection configurations were used depending on the measurement purpose.

The time-integrated PL measurements were performed under non-resonant continuous wave (cw) excitation at low average power densities of 4 to 3000 W/cm^2 using a frequency doubled Nd:YAG laser at 2.33 eV(532 nm), a He-Ne laser at 1.96 eV (633 nm) and a Ti:Sapphire laser at 1.59 eV (780 nm). The temperature dependent PL spectra of the 4 ML QDot sample and all QDash samples were measured using a 75-cm monochromator with a 300 groves/mm grating and a liquid Nitrogen cooled InGaAs photodiode array detector. For the 6 ML QDot sample, a slightly modified detector set-up was used because the PL energy exceeded the cut-off wavelength (1.6 μm) of the above mentioned detector. A 30-cm monochromator with a rotating 200 groves/mm grating and a liquid nitrogen cooled InGaAs photodiode detector with an extended sensitivity range up to 2.2 μm were used in lock-in operation with the excitation laser being modulated by a mechanical chopper.

The time-resolved PL measurements were performed with ~5 ps pulses with a repetition rate of 76 MHz generated by mode locked Ti:Sapphire laser at 1.59 eV (780 nm). A 150 groves/mm monochromator and a streak camera were used for the detection of the time-resolved PL spectra.

IV. TIME-INTEGRATED PL MEASUREMENTS

A. Low temperature PL spectra

The CW time-integrated measurements were performed and the low temperature PL spectra of an ensemble of 4 ML InAs QDots embedded in $In_{0.53}Al_{0.22}Ga_{0.25}As$ barriers and an ensemble of 4 ML InAs QDashes in $In_{0.52}Al_{0.48}As$ barriers are displayed in Figs. 3(a) and 3(b), respectively. The optical signatures of the QDots, the barrier, and the substrate are highlighted in Fig. 3(a), where the solid line (red) corresponds to the PL measured using the YAG laser of 4 W/cm^2 and the solid filled (blue) area corresponds to the PL recorded under the higher excitation power of 180 W/cm^2 using the He-Ne laser. The PL from the 4 ML QDots is observed at around 0.885 eV (1.401 μm), which is 258 meV below the barrier and 540 meV below the substrate emission. In contrast to the previous report,[49] no WL emission is observed from our QDot samples even under the higher excitation.

In Fig. 3(b), the PL spectra observed from the 4 ML QDash sample are shown in a similar way to the QDot, where the solid line (red) is the PL measured using the YAG laser of 4 W/cm^2 and the solid filled (green) area is the PL measured using the He-Ne laser of 180 W/cm^2. The red-shift of the QD lower energy emission band in both cases is due to the band gap renormalization in QDs.[50] In stark contrast to the QDot samples, the QDash samples exhibit WL emission along with barrier, substrate, and QDash PL. The 4 ML QDash PL

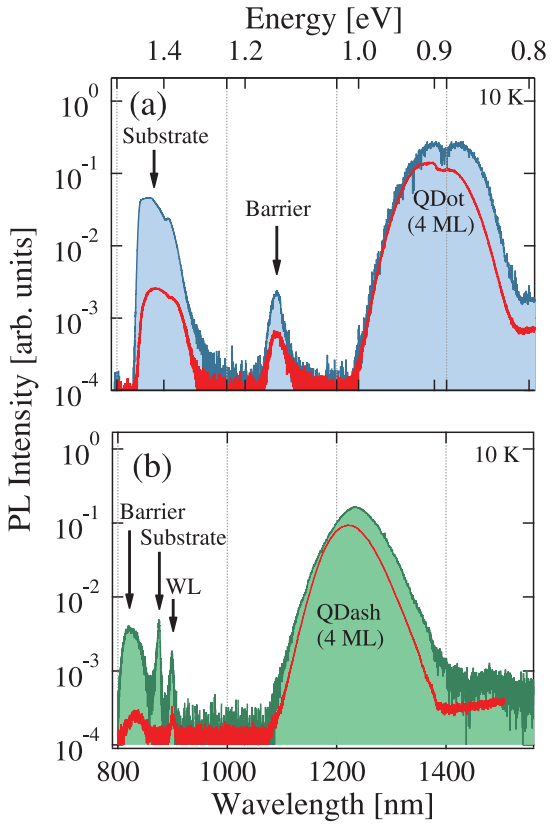

FIG. 3. (a) Low temperature PL spectrum of 4 ML InAs/$In_{0.53}Al_{0.22}Ga_{0.25}As$ QDots featuring the QDot PL at 0.885 eV (1.401 μm), the barrier emission at 1.142 eV (1.085 μm) and the substrate emission at 1.425 eV (0.870 μm). The solid line (red) is the PL measured using a YAG laser (2.33 eV) of 4 W/cm^2 and the solid filled (blue area) is the PL recorded under the excitation power of 180 W/cm^2 using He-Ne laser (1.95 eV). (b) Low temperature PL spectrum of 4 ML InAs/$In_{0.52}Al_{0.48}As$ QDashes measured in a similar way using the YAG laser (2.33 eV) of 4 W/cm^2 (the solid red line) and using He-Ne laser (1.95 eV) of 180 W/cm^2 (the solid filled green area) featuring the QDash PL at 1.005 eV (1.233 μm) as well as emission from the WL (1.377 eV; 0.900 μm), substrate (1.425 eV; 0.870 μm) and barrier (1.53 eV; 0.810 μm).

emerges at around 1.005 eV (1.233 μm), which is 372 meV below the WL, 420 meV below the substrate and 525 meV below the barrier emission.

B. Temperature dependent PL analysis

The normalized low-temperature PL spectra of 4 and 6 ML QDots are shown in Fig. 4(a). By increasing the QDots effective deposition thickness from 4 to 6 ML, the PL peak shows the red-shift to 0.800 eV (1.550 μm), the desired emission range for usage in silica fiber networks; accordingly, the energy separation between QDots and barrier increases from 258 to 342 meV. The QDot PL temperature dependence was investigated and exemplarily the PL spectra of the 4 ML QDots at different temperatures between 10 and 250 K are displayed in Fig. 4(b). The QDot PL successively red shifts with increasing temperature and eventually quenches.

The integrated intensity of the 4 ML and 6 ML QDot PL is semi-logarithmically plotted against the inverse temperature in Fig. 4(c). It is almost constant up to 40 K and exhibits a soft reduction of PL between 40 and 120 K. Above 120 K, the intensity starts to diminish rapidly, indicating the presence of rapid non-radiative recombination mechanisms. Previously

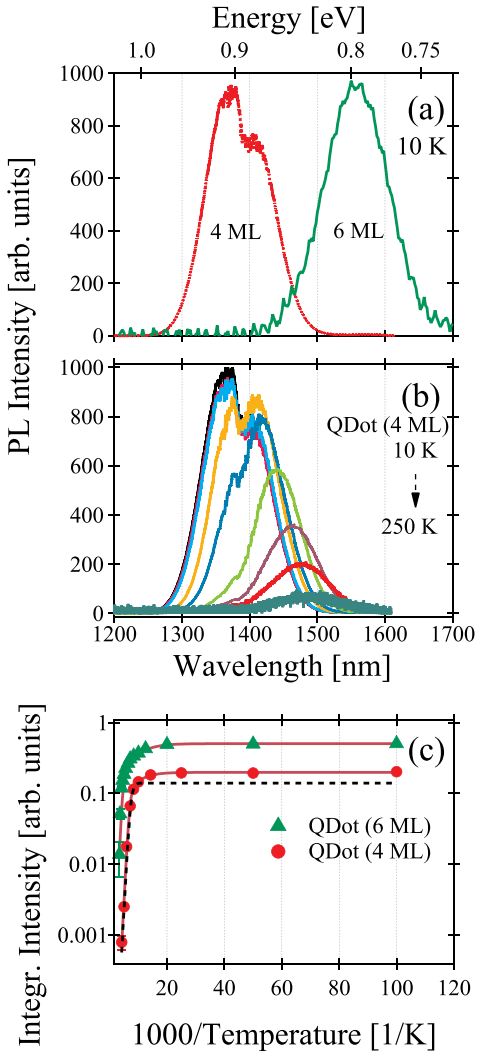

FIG. 4. (a) Low temperature PL spectra of InAs QDots of 4 and 6 ML nominal thickness. (b) Temperature dependent PL spectra of 4 ML QDots at T = 10, 20, 40, 70, 100, 140, 170, 200, and 250 K under low power non-resonant excitation (7 W/cm^2). The "dips" at about 0.89 eV in the 4 ML QDot spectra are due to the OH^- absorption in the fibers used for these measurements. (c) Integrated PL intensities of 4 and 6 ML InAs QDots displayed as a function of inverse temperature. The fit curves (black solid lines) were obtained using Eq. (1). The dashed line corresponds to the line calculated by Eq. (1) with the fixation of the coefficient $B_1 = 0$.

single exponential fits have been studied and initially we also tried in the same way, but clear deviation remained in the fittings. The solid lines in Fig. 4(c) result from the best fit to the experimental data by the Arrhenius-type equation[27,51]

$$I(T) = \frac{I_0}{1 + B_1 \exp\left(-\frac{E_{a1}}{kT}\right) + B_2 \exp\left(-\frac{E_{a2}}{kT}\right)}. \quad (1)$$

I_0 is the integrated PL intensity at 0 K, E_{a1} and E_{a2} are the two thermal activation energies, B_1 and B_2 are the corresponding dimensionless coefficients, k is the Boltzmann constant, and T is the sample temperature. After the fitting, we examined the contributions of the two exponential terms by intentionally setting $B_1 = 0$. This result is shown with the dashed line for the 4 ML QDots in Fig. 4(b). The temperature

TABLE I. Activation energies and fitting coefficients.

	Activation energy		Fitting coefficient	
Sample	E_{a1}(meV)	E_{a2} (meV)	B_1	B_2
4 ML QDots	22 ± 2.2	157 ± 4.8	4.7 ± 0.41	$6.4 \times 10^5 \pm 0.09 \times 10^5$
6 ML QDots	20 ± 1.4	189 ± 6.0	4.3 ± 0.71	$2.4 \times 10^4 \pm 0.06 \times 10^4$
3 ML QDashes	25 ± 3.0	180 ± 7.3	4.4 ± 0.51	$4.8 \times 10^5 \pm 0.09 \times 10^5$
4 ML QDashes	17 ± 2.0	224 ± 5.8	2.8 ± 0.36	$2.4 \times 10^6 \pm 0.05 \times 10^6$
6 ML QDashes	19 ± 2.8	275 ± 3.7	3.4 ± 0.57	$1.7 \times 10^7 \pm 0.04 \times 10^7$

range higher than 120 K remains well fitted but the difference appears in the lower temperature range. This clearly shows that the B_1 term with the smaller activation energy of E_{a1} represents the slow PL quenching in the lower temperature range. The parameters derived from the fittings on the 4 and 6 ML QDots are summarized in Table I.

The PL of InAs QDashes was investigated as a function of temperature in a comparable way to the QDots and is displayed in Fig. 5. The low temperature spectra of 3, 4, and 6 ML QDash samples are shown in Fig. 5(a) and their PL is centered at about 1.13 eV (1.095 μm), 1.005 eV (1.233 μm), and 0.861 eV (1.440 μm), respectively. This implies that also the QDash emission exhibits the increasing energy separation from the WL, barrier, and substrate with increasing QDash MLs. Exemplarily for the QDash PL temperature dependence, the 4 ML QDash spectra between 10 and 293 K are displayed in Fig. 5(b). The integrated PL intensities of all three QDash ensembles are plotted similarly as a function of inverse temperature in Fig. 5(c). The experimental best-fitted data based on Eq. (1) are summarized in Table I. The contribution of the two activation energies were studied in a similar way to the QDot case and the dashed line calculated by intentionally setting $B_1 = 0$ gives qualitatively the similar result as the QDot case.

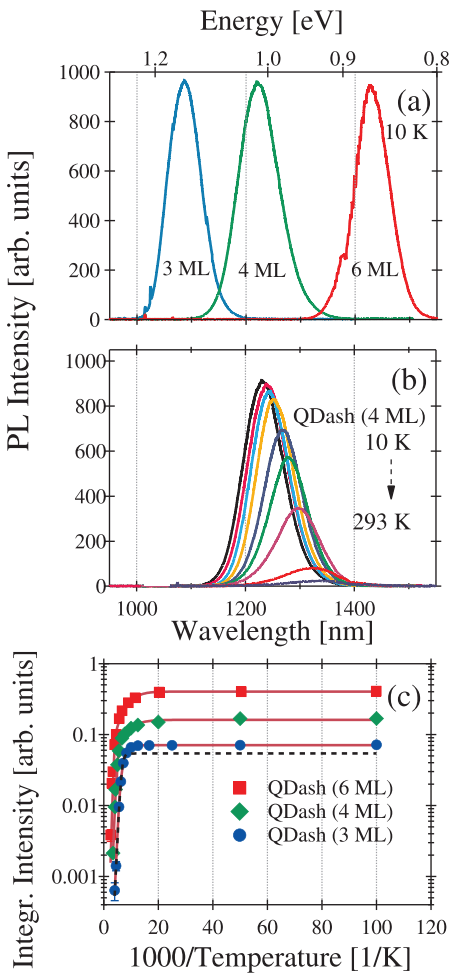

FIG. 5. (a) Low temperature PL spectra of InAs QDashes of 3 to 6 ML nominal thickness. (b) Temperature dependent PL spectra of 4 ML QDashes at T = 10, 50, 80, 100, 120, 140, 180, 240 and 293 K under low power nonresonant excitation (13 W/cm^2). (c) Integrated PL intensities of the 3, 4 and 6 ML InAs QDashes displayed as a function of inverse temperature. The fit curves (black solid lines) were obtained using Eq. (1). The dashed line represents the line calculated using Eq. (1) by fixing $B_1 = 0$.

Table I summarizes the activation energies, fitting coefficients and the one-standard deviation fit errors of all the investigated QDot and QDash samples. A detailed discussion of the fit parameters, especially the energies and the related escape processes, is carried out in the subsequent sections.

C. Discussions

1. Coefficients $B_{1,2}$

The fitting coefficients $B_{1,2}$ listed in Table I are defined simply as the ratio of carrier capture time of the QDs and carrier escape time of the QDs by the respective nonradiative process, which is narrated in a distinctive manner by Le Ru *et al.*[52] Consequently, a scenario with a significantly faster carrier capture than escape time leads to small values of $B_{1,2}$ and vice versa. From the experimental results of both samples, it is obvious that the values of B_1 are significantly smaller than those of B_2. Hence, in case of similar magnitudes of the related exponential functions, the term scaled by B_2 is the dominating contribution to the thermally activated charge carrier escape process, while the term scaled by B_1 plays a minor role.

2. Activation energy E_{a2}

First, we discuss the mechanism behind the larger activation energies E_{a2}. The following ratio:

$$\nu_i = E_{a2,i}/\Delta E_i, \quad \text{or} \quad E_{a2,i} = \nu_i \Delta E_i \tag{2}$$

is introduced, where the "optical energy gap" ΔE_i is the transition energy difference of the QDs and any associated higher energy state (e.g., the barrier or WL) which is designated by the index i. The ratio in Eq. (2) classifies three different scenarios of charge carrier escape. For $\nu_i \cong 1$, an escape process of excitons is described.[39] For $\nu_i \cong 0.5$, an escape process is described where $E_{a2,i}$ is half of the ΔE_i. According to Yang *et al.*[40] and Michler *et al.*,[53] this condition is derived for an escape process of electrons and holes with equal probability. This situation is most probable when the band discontinuities in the conduction and valence bands are similar, and the electron and hole concentrations are equal. For $\nu_i < 0.5$, the escape is dominated by single charge carrier escape with $E_{a2,i}$ corresponding to the less confined

charge carriers due to the smaller discontinuity of either conduction or valance band.

To compare our experimental results with the above mentioned escape mechanisms, the activation energies of QDots and QDashes are displayed in Fig. 6 with respect to their corresponding number of MLs. The blue diamond's (red circles) represent the QDashes (QDots) activation energies in Fig. 6. The blue solid line is the fitting of $\nu_i \Delta E_i$, where ΔE_i is given by the energy difference between the QDashes emission peak energy and the WL emission energy. For the QDot samples, WL emission was not observed as shown in Fig. 3(a). Therefore, ΔE_i is given by the energy difference between the QDots emission peak energy and the barrier emission energy, assuming the absence of WL in the QDot sample, and the fit to the measured E_{a2} values is shown by the red solid line. As is discussed in Sec. IV C 4 both the QDash and QDot PL peaks show the additional red-shift of ~25 meV due to carrier re-distribution within QDashes in the temperature range $\sim 40\,\mathrm{K} < \mathrm{T} < \sim 140\,\mathrm{K}$. Since E_{a2} is obtained from the fitting in this higher temperature range, this red-shift was added in the ΔE_i values.

The reasonable fitting with Eq. (2) (not shown here) was possible with $\nu_i = 1/2$, indicating that the escape of correlated electron-hole (e-h) pair is dominating. However, better fitting is possible by slightly increasing the ν_i value from 0.5 as shown in Fig. 6. The resultant ν_i values are 0.63, 0.56, and 0.51 for the 3, 4, and 6 ML QDash samples, and 0.54 and 0.51 for the 4 and 6 ML QDot samples, respectively. This slight increase of the ν_i value will be probable with the involvement of the exciton escape mechanism as well. It is known that excitons are stable at the lower temperature but dissociate at higher temperature. Therefore, partially survived excitons will escape in the intermediate temperature range and this will increase the ν_i value slightly from 0.5. Smaller QDs normally show the larger OS than the larger ones due to enhanced quantum confinements and the OS variation which is discussed later in Sec. V based on our measurements. Therefore, the observed larger ν_i values for the smaller QDs are rational considering the higher contribution

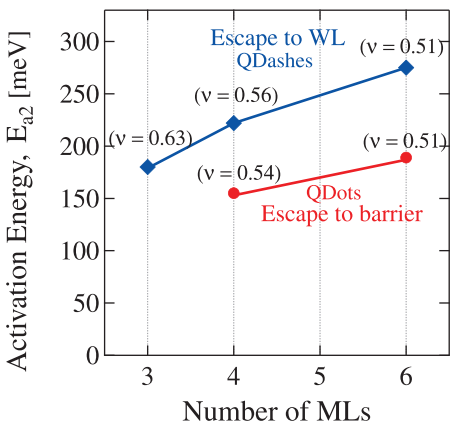

FIG. 6. Activation energies of QDots and QDashes as a function of their number of MLs (height); blue diamonds represent the QDashes, red circles the QDots. The blue (red) solid line represents the multiplication of ν_i with ΔE_i (ΔE_i = the energy separation between the QDash (QDot) PL and the WL (barrier) PL, deduced at high temperatures including the additional PL peak shift described below in Sec. IV C 4).

of the exciton mechanism. The validity of these ν_i values will be further re-examined in Sec. V with the measurements of excited-state and ground-state energy differences.

It is noted that the nice fitting in Fig. 6 was obtained by assuming the carrier escape to the barrier layer for the QDot samples due to the absence of WL PL as shown in Fig. 3(a). Previously dominant WL-PL emission was reported at 0.99 eV for InAs/InP(311)B QDs by Hinooda *et al.*[49] If we assume the presence of the same WL, latent in our samples, then the energy difference between the center of the luminescence peaks of the 4 ML QDots and that latent WL will be 104 meV. This results in $\nu_i = 1.51$ using Eq. (2). This is not realistic and cannot corroborate any of the escape mechanism described by Eq. (2). This strongly suggests that there is no WL in our QDot samples.

3. Activation energy E_{a1} and thermally assisted exciton transfer

The values of the smaller activation energy E_{a1} range from 20 to 22 meV for the 4 to 6 ML InAs/InGaAlAs QDots and from 17 to 25 meV for the 3 to 6 ML InAs/InAlAs QDashes (Table I). From the similarity of these values, we can infer that the value of E_{a1}, and thus the related escape process, is almost independent of the barrier material as well as QD symmetry. The mechanism related with this small activation energy cannot be directly connected to an energy gap because it is too small to activate carriers to the WL or barrier from the QD ground states (GS). It is rather close to the energy separation of the QD GS and the excited states.[54]

For arrangements of QDs with small separations, various types of charge carrier or exciton tunneling have been discussed, including the role of excited states. For example, a carrier thermal escape and re-trapping model connecting barriers, WL, and QDs were discussed in Ref. 26 which takes into account the random carrier capture by QDs, absence of direct tunneling among QDs, and the role of WL to provide a channel for carrier exchange. Non-resonant phonon-assisted tunneling of holes between QDs in adjacent stacked layers through coupled excited states (CES) in the valence-band was also discussed in Ref. 55. On the other hand, non-resonant exciton tunneling between laterally coupled QDs in single lateral QD molecules (connected through basin) was discussed, with the focus on the most likely transitions between indirect and direct excitons, which correspond to an effective hopping of the electron.[56] These two reports are dealing with the coupling of QD GS with small QD spacing.

Areal density usually decides the strength of interaction between adjacent QDs which can be viewed as the signature of lateral coupling. In our present highly dense QDs system close to $\sim 10^{11}\,\mathrm{cm}^{-2}$, the average QD spacing is 2–6 nm as estimated in Sec. II. This distance is larger than the laterally coupled QDs[55,56] and the direct tunneling between the GS of neighboring QDs may be impeded. However, the CES is much more probable because of the larger extensions of the excited-state wave functions. The relation of the resultant quasi-continuous CES and the GS of typical small and large QDs, together with the WL and the barrier energies, is illustrated with the excitonic-energy schematic diagram in Fig. 7.

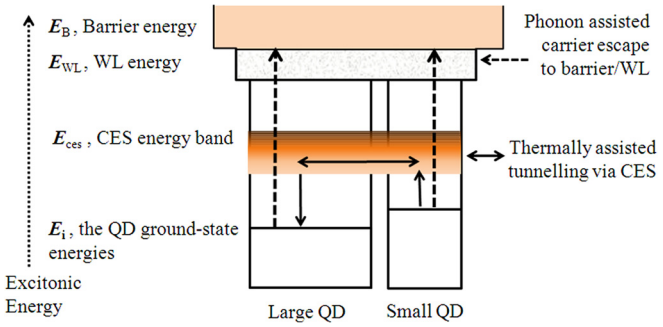

FIG. 7. Schematic illustration of the thermal escape and charge carrier redistribution model exemplifying two QDs of different size and GS energy and the related thermally activated carrier escape and tunneling processes between QDs, as well as the common features CES, barrier (for QDot samples) and WL (for QDash samples).

Possible charge carrier transfer processes are depicted with the arrows in Fig. 7. Thus, it becomes possible that the charge carriers (correlated electron-hole pair) in the small QD GS are thermally activated and transferred to the larger QD GS via CES.

Khatsevich *et al.* showed that thermal escape processes could be more precisely discussed by focusing to the relation between the difference of the thermal activation energies from the QD GS and excited states and the difference of the QD GS and excited state energies.[39] It is expressed by the following equation:

$$E_{a(GS)} - E_{a(exc)} = \nu_i \Delta E_{GS\text{-}Exc}, \quad (3)$$

where $E_{a(GS)}$ and $E_{a(exc)}$ are the respective thermal activation energies from the QD GS and excited states, $\Delta E_{GS\text{-}Exc}$ is the energy difference between the transition energies of QD GS and excited states, and ν_i is the ratio appeared in Eq. (2).

We apply this concept to our inter-dot carrier transfer process. Based on the above-discussed model, the left-hand side of Eq. (3), $E_{a(GS)} - E_{a(exc)}$, in this case is equivalent to the measured E_{a1} shown in Table I. The values of $\Delta E_{GS\text{-}Exc}$ are determined from the ensemble envelope of QD PL spectra observed at increased excitation powers on the QDot/QDash samples prepared in sub-μm-diameter mesa structures. One of the PL results is shown in Sec. IV (Fig. 10(b)). For 3, 4, and 6 ML QDashes $\Delta E_{GS\text{-}Exc}$ is determined as 42.2, 40.4, and 36.8 meV, while for 4, and 6 MLs QDots is extracted as 41.3, and 39.2 meV, respectively. Employing the values of ν_i, derived from the fitting to E_{a2} shown in Fig. 6, in the right hand side of Eq. (3), we obtain the following results:

6 ML QDash, $E_{a1} = E_{a(GS)} - E_{a(exc)} = \nu_i \Delta E_{GS\text{-}Exc} = 0.51 \times 36.8\,\text{meV} = 18.8\,\text{meV}$, measured (19 meV)
4 ML QDash, $E_{a1} = E_{a(GS)} - E_{a(exc)} = \nu_i \Delta E_{GS\text{-}Exc} = 0.56 \times 40.4\,\text{meV} = 22.6\,\text{meV}$, measured (17 meV)
3 ML QDash, $E_{a1} = E_{a(GS)} - E_{a(exc)} = \nu_i \Delta E_{GS\text{-}Exc} = 0.63 \times 42.2\,\text{meV} = 26.5\,\text{meV}$, measured (25 meV)
6 ML QDots, $E_{a1} = E_{a(GS)} - E_{a(exc)} = \nu_i \Delta E_{GS\text{-}Exc} = 0.51 \times 39.2\,\text{meV} = 20\,\text{meV}$, measured (20 meV)
4 ML QDots, $E_{a1} = E_{a(GS)} - E_{a(exc)} = \nu_i \Delta E_{GS\text{-}Exc} = 0.54 \times 41.3\,\text{meV} = 22.3\,\text{meV}$, measured (22 meV)

Except for the 4 ML QDash sample, the measured E_{a1} is well explained with the ν_i values determined in Sec. IV. This demonstrates that the inter-dot carrier transfer also supports the correlated electron-hole pair escape model. This carrier transfer from the smaller QDs to the larger QDs is consistent with the QD PL peak red-shift shown in Fig. 8 for $\sim$40 K $<$ T $<\sim$140 K and the increase of the lifetime shown in Fig. 9(b) for T $<$ 140 K. The details will be discussed in the subsequent sections.

4. Temperature-dependent QD repopulation and PL red-shift

To provide a clearer picture of the inter-QD tunneling and charge carrier redistribution we take another close look on the above presented PL data (Figs. 4 and 5), especially on the temperature dependence of the PL peak energy and line width. Exemplarily, 4 ML QDots and QDashes are selected for the following discussion. Figures 8(a) and 8(c) illustrate the temperature dependence of the luminescence peak energy of 4 ML QDots and QDashes, respectively. The respective PL peak energies were extracted from the PL temperature dependence shown in Figs. 4 and 5 by the Gaussian line-shape fitting and the temperature dependence is compared with the Varshni empirical expression,

$$E(T) = E_0 - \frac{\alpha T^2}{\beta + T}, \quad (4)$$

where E_0 is the 0 K energy gap, T is the temperature, and α and β are the fitting parameters known for bulk InAs. For the best fit of Eq. (4), the observed temperature dependence is fitted from the low-temperature and high-temperature limits. The two green dashed lines are the calculated temperature dependences, which highlight the relative energy changes.

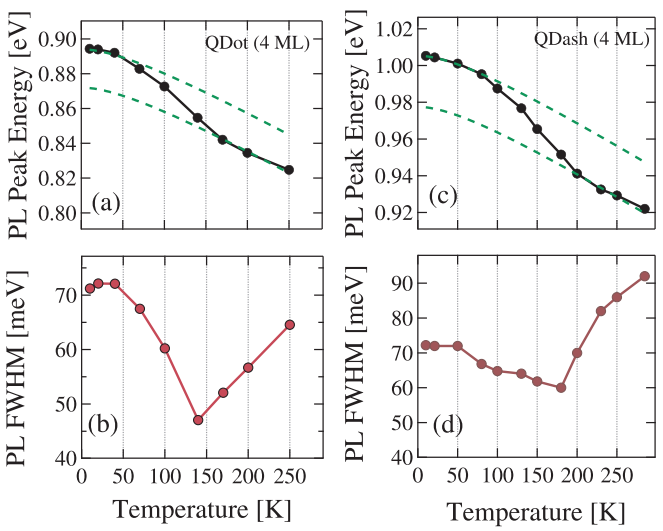

FIG. 8. (a) Temperature dependence of the 4 ML QDot PL obtained from Gaussian fits to the spectra (Fig. 4). The two parallel dashed lines are calculated using Eq. (4) ($\alpha = 0.27$ meV/K and $\beta = 94$ K).[57] (b) Temperature dependence of the 4 ML QDot PL FWHM obtained from Gaussian fits to the spectra. (c) Temperature dependence of the 4 ML QDash PL extracted from Gaussian fits to the spectra (Fig. 5); displayed in the same way as in (a). (d) Temperature dependence of the 4 ML QDash PL FWHM.

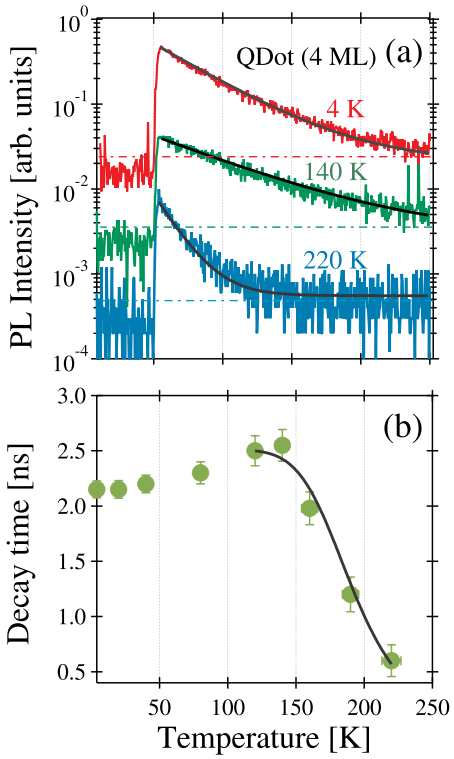

FIG. 9. (a) Time-resolved PL of 4 ML QDots as a function of temperature (4, 140, and 220 K) under low power non-resonant excitation (25 W/cm^2). The transients were obtained by spectrally binning the data between 1.3–1.5 μm, 1.325–1.525 μm, and 1.350–1.550 μm, respectively. The solid lines are the results of single-exponential fits. The horizontal dashed lines are guide to the eyes to show the offset noise level. (b) Temperature dependence of the decay time, the solid line represents the resultant fit to the higher temperature data points obtained by Eq. (9).

This comparison clearly unveils that the PL peak energies of both samples show the enhanced red-shift at intermediate temperatures between about 40 and 140 K.[27,38] Similar red-shifts have also been observed for the other samples of different QD sizes that have been discussed earlier in this work (not shown here). The origin of this additional red-shift of the PL peak energy is explained by the charge carrier redistribution via the transfer from high-energy smaller-sized QDs to low-energy lager-sized QDs via the CES.

In Fig. 8(b), a decrease of the 4 ML QDot PL line width (full width at half maximum, FWHM) is observed between 40 and 140 K. The FWHM of the 4 ML QDot ensemble PL reduces by ~35% with temperature and reaches its minimum at 140 K. For higher temperatures, the FWHM again starts to increase, which is attributed to various broadening mechanisms such as electron-phonon interactions.[58] A similar reduction of the FWHM is found between 50 and 180 K for the 4 ML QDashes (Fig. 8(d)). This clear trend of a FWHM reduction with increasing temperature coincides well with the observed PL peak shift and also supports the suggestion of charge carrier redistribution from high to low energy QDs.

V. TIME-RESOLVED PL MEASUREMENTS AND TEMPERATURE DEPENDENCE OF DECAY TIME

Another obvious approach to investigate charge carrier dynamics in QDs and thermally activated escape processes is the direct measurement of dynamic processes, e.g., by using transient spectroscopy. Time-resolved PL spectroscopy as a function of temperature was performed on the QDot and QDash samples with similar results. In the following the 4 ML QDot results are presented and discussed exemplarily. As introduced in Sec. III, a streak camera was used to detect the PL under non-resonant excitation with ps-laser pulses. Post measurement accumulation of the PL counts within a suitable selected wavelenth range was performed to obtain the transient PL as a function of temperature and excitation power. The transients taken at 4, 140, and 220 K under low excitation power (25 W/cm^2) are displayed in Fig. 9(a). The single-exponential fitting of the experimental data results in a lifetime of 2.16 ns at 4 K which is attributed to the radiative decay of QDot GS excitons, since a measured decay can be assumed as a purely radiative decay at low temperature below 10 K.[35] The PL lifetime versus temperature, depicted in Fig. 9(b), indicates that at low temperatures between 4 and 40 K the lifetime of 2.16 ns remains nearly constant while it increases up to 2.56 ns at the intermediate temperatures between 40 and 140 K. The temperature range of this life time increase coincides with the PL line width reduction, which is another indication of the charge carrier redistribution as discussed in the previous section. Related thermalization of charge carriers among differently sized InAs/GaAs QDs was reported by Rainò *et al.*[59] and is accountable for the lasing line width narrowing and the increase of lasing efficiency at high temperature.[60] At the higher temperature above 140 K, a steep reduction of the lifetime is observed. The observed temperature dependence will be quantitatively analysed in the following.

For the temperature up to 140 K, the measured decay time as shown in Fig. 9(b) increases while the integrated PL intensity shown in Fig. 4 decreases. The relation of these behaviors is quantitatively studied considering the carrier transfer from the smaller QDots to the larger QDots via the QD CES shown in Fig. 7. As the representative measured data, let us compare the measured values at 4 K and 120 K. The measured ratio is given as

$$R_{\mathrm{PL}} \equiv \frac{I_{\mathrm{PL}}(120\,\mathrm{K})}{I_{\mathrm{PL}}(4\,\mathrm{K})} = 0.86,$$
$$R_{\tau} \equiv \frac{\tau_{\mathrm{decay}}(120\,\mathrm{K})}{\tau_{\mathrm{decay}}(4\,\mathrm{K})} = \frac{2.50\ (\mathrm{ns})}{2.16\ (\mathrm{ns})} = 1.15. \tag{5}$$

The integrated PL intensity is proportional to the internal quantum efficiency η_{eff}, and η_{eff} is related to the radiative lifetime τ_{rad} and non-radiative lifetimes τ_{nonrad} with the following equation:

$$\eta_{\mathrm{eff}} = \frac{1/\tau_{\mathrm{rad}}}{1/\tau_{\mathrm{rad}} + 1/\tau_{\mathrm{nonrad}}} = \frac{\tau_{\mathrm{decay}}}{\tau_{\mathrm{rad}}}. \tag{6}$$

Then from Eq. (5),

$$R_{\mathrm{PL}} = \frac{\eta_{\mathrm{eff}}(120\,\mathrm{K})}{\eta_{\mathrm{eff}}(4\,\mathrm{K})} = \frac{\tau_{\mathrm{decay}}(120\,\mathrm{K})}{\tau_{\mathrm{rad}}(120\,\mathrm{K})}\frac{\tau_{\mathrm{rad}}(4\,\mathrm{K})}{\tau_{\mathrm{decay}}(4\,\mathrm{K})}$$
$$= R_{\tau}\frac{\tau_{\mathrm{rad}}(4\,\mathrm{K})}{\tau_{\mathrm{rad}}(120\,\mathrm{K})}. \tag{7}$$

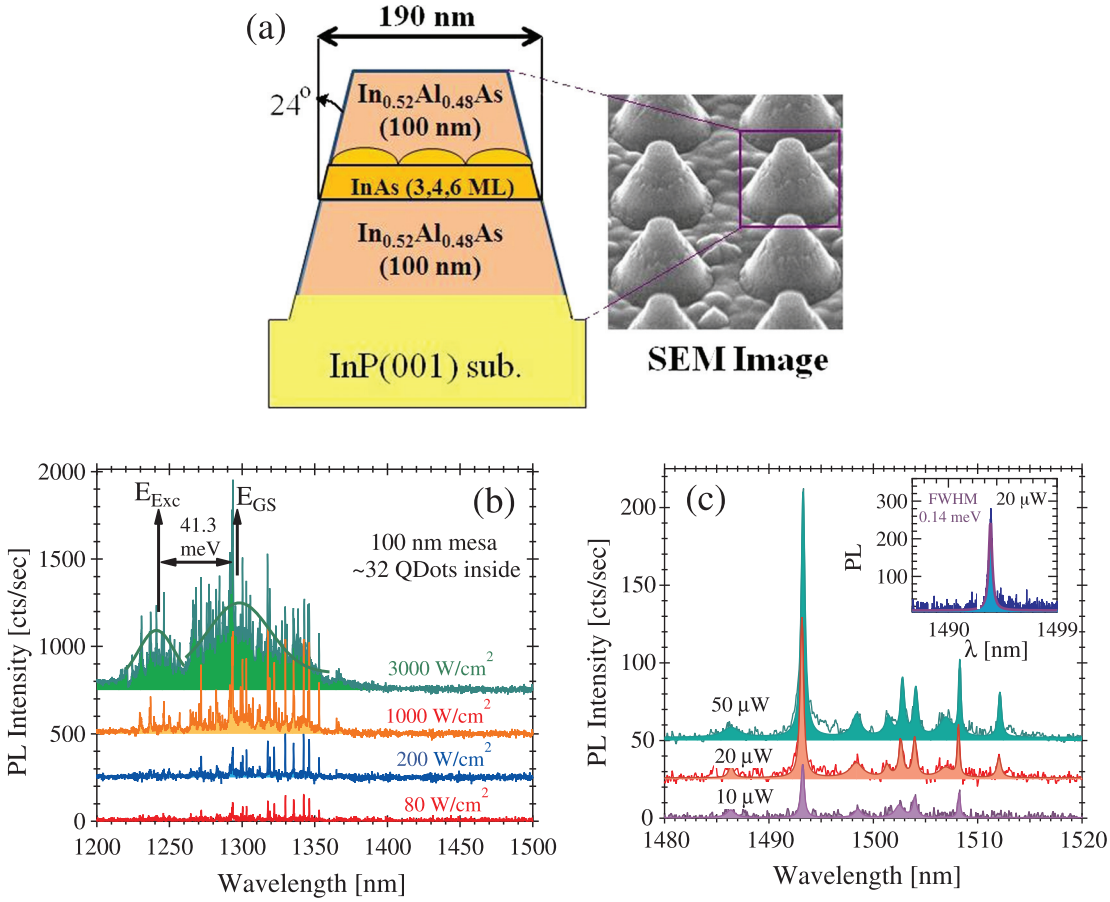

FIG. 10. (a) Schematic illustration of a 190 nm sized mesa and the corresponding secondary-electron microscope (SEM) image with a 24° taper angle, a height of 230 nm and a top diameter of 100 nm. (b) Low temperature (4 K) excitation power dependence of μ-PL spectra of few no. of 4 ML QDots embedded in a mesa of top diameter of 100 nm. With increased excitation power emission from excited states is also taking place. (c) Low temperature (4 K) excitation power dependence of high resolution μ-PL spectra of single 6 ML QDashes embedded in a 190 nm mesa, featuring emission lines from a few individual QDashes emitting near the telecommunication C band. The FWHM is Lorentzian and found around 140 μeV.

The temperature dependent variation of the radiative lifetime is calculated from Eq. (7). Since the oscillator strength (OS) for the inter-band optical transition is inversely proportional to the radiative lifetime, the temperature dependent change of the OS is estimated as

$$R_{\mathrm{O.S.}} \equiv \frac{\mathrm{O.S.(120\,K)}}{\mathrm{O.S.(4\,K)}} = \frac{\dfrac{1}{\overline{\tau_{\mathrm{rad}}(120\,\mathrm{K})}}}{\dfrac{1}{\overline{\tau_{\mathrm{rad}}(4\,\mathrm{K})}}} = \frac{R_{\mathrm{PL}}}{R_{\tau}} = 0.75. \quad (8)$$

The reason why the average radiative lifetime, that is the OS, changes with temperature is because of the carrier redistribution takes place from the smaller QDots with the larger OS to the larger QDots with the smaller OS via the transfer through the CES for the higher temperature. It has been previously reported that larger QDs generally exhibit smaller OS than smaller QDs.[61,62] The temperature variation of the radiative lifetime changes the relative contribution of the residual nonradiative recombination in Eq. (6) and therefore the increase of the radiative lifetime slowly quenches the PL intensity for the temperature rise up to ~140 K.

At the higher temperature above 140 K, the steep reduction of the lifetime is observed in Fig. 9(b). Both the steep reduction of the PL integrated intensity shown in Fig. 4(c) and the decrease of the lifetime are attributed to the dominant correlated electron-hole carrier escape to the barrier layers for the QDot samples (carrier escape to the WL for the QDash samples). The following equation is used to extract the activation energy from the lifetime versus temperature plot in the high temperature regime.[63]

$$\tau(T) = \frac{\tau_d}{1 + \dfrac{\tau_d}{\tau_E}\exp^{-E_a/k_B T}}, \quad (9)$$

where T is the temperature and k_B is the Boltzmann constant. τ_d is the decay time at the low-temperature limit and is fixed to 2.5 ns based on the measurement shown in Fig. 9(a) at the intermediate temperature. The activation energy E_a and the escape time of charge carriers to the QDot barrier, τ_E, are the fitting parameters. The fitting to the measured data shown by the solid line in Fig. 9(b) results in the activation energy E_a of 150 ± 10 meV, which is close to the activation energy of 157 meV derived from the temperature dependent time-integrated intensity for this 4 ML QDot sample shown in Table I. The escape time τ_E of 10 ± 3 ps is obtained from the fitting, suggesting the significant carrier escape in accordance with the reported non-radiative lifetime in QDs in the range of several picoseconds.[64]

VI. SINGLE QDOT AND QDASH PL

In the final step, we aimed for realizing a practical way to address single QDashes with PL energies of around 0.8 eV (1.55 μm). Recently, Takemoto *et al.* reported ten times enhanced extraction efficiency from QDs embedded in 22° tapered macroscopic horn structure compared to bare self-assembled QDs.[65] Following this, tapered sub-μm sized mesa structures with approximately 200 to 300 nm height and diameters of down to 190 nm (Fig. 10(a))[28,66] were fabricated by using electron beam lithography and reactive ion etching in order to extract single QD emission from the high density samples. We performed micro-PL measurement of a few QDashes embedded in a nm-sized mesa with a diameter of 190 nm of the QDash-containing plane under non-resonant excitation and at cryogenic temperature of 4 K. We selected the 6 ML QDashes to provide about 1.55 μm photons suitable for low loss fiber optical communication in C band, with the capability to be used at elevated temperatures, e.g., liquid Nitrogen temperature of 77 K. We also used the 4 ML QDots to provide photon emission at around 1.3 μm for O band optical communication as well. We successfully demonstrate single QDot and QDash emission at about 1.3 μm (Fig. 10(b)) and at around 1.51 μm (Fig. 10(c)) which takes us a step forward to using these QDots and dashes for quantum optical applications on the single dot/dash level in the telecommunication band.

VII. SUMMARY AND CONCLUSIONS

The PL of high density InAs QDots and QDashes grown on different InP substrates was investigated. Almost circular QDots with PL between 1.2 and 1.6 μm were grown on InP(311)B substrates without the formation of a WL. In contrast, elongated dots or QDashes with PL between 1 and 1.55 μm were grown on InP(001) substrates including the formation of a WL. Temperature dependent time-integrated and time-resolved PL spectroscopy were performed to investigate the charge carrier recombination, transfer and escape mechanisms, as well as the inter-QD coupling; conclusive results could be obtained for the different measurements of all samples. Moreover, a model was used to describe these processes, which includes two different contributions to the thermal quenching which are dominant in the low and high temperature regimes. It could be demonstrated that the mechanism associated with the larger activation energies of around 157–275 meV, depending on the sample, is the dominating PL quenching at higher temperatures; the energies coincide with almost half of the energy difference between QDot (QDash) emission and barrier (WL) emission, which is attributed to the correlated electron-hole pair escape.

The second common escape mechanism corresponds to the smaller activation energy of around 20–25 meV. This mechanism is due to the charge carrier transfer from high-energy smaller QD GS to low-energy larger QD GS via the tunneling through the CES. With the measured excite-state and GS energy differences, the inter-dot charge carrier transfer also supports the correlated electron-hole pair escape. This resulted in the re-distribution of the charge carriers among the QDs. The relation to the slow PL intensity quenching and increase of the decay time for the temperature rise up to ~140 K was quantitatively well explained with the QD-size dependent variation of the QD oscillator strength. Finally, we suggest and demonstrate a way to access individual 6 ML QDashes by embedding them in nm-sized mesas. We successfully demonstrated photon emission close to 1.55 μm from individual QDashes. In this way we also present a suitable approach to use high density QDashes as attractive sources of single photons for application in future fiber-based quantum communication.

ACKNOWLEDGMENTS

This work was partially supported by the Grand-in-Aid for Scientific Research (S), No. 24226007, Nanotechnology Platform by the Ministry of Education, Culture, Sports, Science and Technology, and SCOPE (Strategic Information and Communications R&D Promotion Programme) from the Ministry of Internal Affairs and Communications, Japan. C.H. acknowledges the Japan Society for the Promotion of Science (JSPS) for providing financial support in the form of a JSPS Fellowship for Foreign Researchers; N.A.J. acknowledges financial support via a MEXT scholarship.

[1]P. Caroff, C. Paranthoen, C. Platz, O. Dehaese, H. Folliot, N. Bertru, C. Labbé, R. Piron, E. Homeyer, A. Le Corre, and S. Loualiche, Appl. Phys. Lett. **87**, 243107 (2005).
[2]R. Nötzel, S. Anantathanasarn, R. P. J. van Veldhoven, F. W. M. van Otten, T. J. Eijkemans, A. Trampert, B. Satpati, Y. Barbarin, E. A. J. M. Bente, Y.-S. Oei, T. de Vries, E.-J. Geluk, B. Smalbrugge, M. K. Smit, and J. H. Wolter, Jpn. J. Appl. Phys. Part 1 **45**, 6544 (2006).
[3]C. Gilfert, V. Ivanov, N. Oehl, M. Yacob, and J. P. Reithmaier, Appl. Phys. Lett. **98**, 201102 (2011).
[4]R. Schwertberger, D. Gold, J. P. Reithmaier, and A. Forchel, IEEE Photon. Technol. Lett. **14**, 735 (2002).
[5]S. Farad, Z. Wasilewski, J. McCaffrey, S. Raymond, and S. Charbonneau, Appl. Phys. Lett. **68**, 991 (1996).
[6]H. Saito, K. Nishi, and S. Sugou, Appl. Phys. Lett. **78**, 267 (2001).
[7]M. Pelton and Y. Yamamoto, Phys. Rev. A **59**, 2418 (1999).
[8]E.-T. Kim, A. Madhukar, Z. Ye, and J. C. Campbell, Appl. Phys. Lett. **84**, 3277 (2004).
[9]P. Michler, A. Kiraz, C. Becher, W. V. Schoenfeld, P. M. Petroff, L. D. Zhang, E. Hu, and A. Imamoglu, Science **290**, 2282 (2000).
[10]Y. Yuan, B. E. Kardynal, R. M. Stevenson, A. J. Shields, C. J. Lobo, K. Cooper, N. S. Beattie, D. A. Ritchie, and M. Pepper, Science **295**, 102 (2002).
[11]C. Santori, D. Fattal, J. Vuckovic, G. S. Solomon, and Y. Yamamoto, Nature **419**, 594 (2002).
[12]R. J. Young, R. M. Stevenson, P. Atkinson, K. Cooper, D. A. Ritchie, and A. J. Shields, New J. Phys. **8**, 29 (2006).
[13]N. Akopian, N. A. Lindner, E. Poem, Y. Berlatzky, J. Avron, D. Gershoni, B. D. Gerardot, and P. M. Petroff, Phys. Rev. Lett. **96**, 130501 (2006).
[14]R. Hafenbrak, S. M. Ulrich, P. Michler, L.Wang, A. Rastelli, and O. G. Schmidt, New J. Phys. **9**, 315 (2007).
[15]B. Alloing, C. Zinoni, V. Zwiller, L. H. Li, C. Monat, M. Gobet, G. Buchs, A. Fiore, E. Pelucchi, and E. Kapon, Appl. Phys. Lett. **86**, 101908 (2005).
[16]M. B. Ward, O. Z. Karimov, D. C. Unitt, Z. L. Yuan, P. See, D. G. Gevaux, A. J. Shields, P. Atkinson, and D. A. Ritchie, Appl. Phys. Lett. **86**, 201111 (2005).
[17]S. Ganapathy, X. Q. Zhang, I. Suemune, K. Uesugi, H. Kumano, B. J. Kim, and T.-Y. Seong, Jpn. J. Appl. Phys. Part 1 **42**, 5598 (2003).
[18]E. S. Semenova, R. Hostein, G. Patriarche, O. Mauguin, L. Largeau, I. Robert-Philip, A. Beveratos, and A. Lemaître, J. Appl. Phys. **103**, 103533 (2008).
[19]M. Strauss, S. Höfling, and A. Forchel, Nanotechnology **20**, 505601 (2009).
[20]J. Brault, M. Gendry, O. Marty, M. Pitaval, J. Olivares, G. Grenet, and G. Hollinger, Appl. Surf. Sci. **162–163**, 584 (2000).

[21]H. Yang, X. Mu, I. B. Zotova, Y. J. Ding, and G. J. Salamo, J. Appl. Phys. **91**, 3925 (2002).
[22]K. Akahane, N. Yamamoto, and M. Tsuchiya, Appl. Phys. Lett. **93**, 041121 (2008).
[23]S. Fréchengues, V. Drouot, N. Bertru, B. Lambert, A. Loualiche, and A. Le Corre, J. Cryst. Growth **201/202**, 1180 (1999).
[24]G. G. Tarasov, Yu. I. Mazur, Z. Ya. Zhuchenko, A. Maaßdorf, D. Mickel, J. W. Tomm, H. Kissel, C. Walther, and W. T. Masselink, J. Appl. Phys. **88**, 7162 (2000).
[25]Yu. I. Mazur, Zh. M. Wang, G. G. Tarasov, M. Xiao, G. J. Salamo, J. W. Tomm, V. Talalaev, and H. Kissel, Appl. Phys. Lett. **86**, 063102 (2005).
[26]S. Sanguinetti, M. Henini, Alessi M. Grassi, M. Capizzi, P. Frigeri, and S. Franchi, Phys. Rev. B **60**, 8276 (1999).
[27]R. Heitz, I. Mukhametzhanov, A. Madhukar, A. Hoffmann, and D. Bimberg, J. Electron. Mater **28**, 520 (1999).
[28]C. Hermannstädter, N. A. Jahan, J.-H. Huh, H. Sasakura, K. Akahane, M. Sasaki, and I. Suemune, New J. Phys. **14**, 023037 (2012).
[29]I. N. Stranski and L. Krastanow, Sitzungsber. Akad. Wiss. Wien, Math.-Naturwiss. Kl., Abt. 2B **146**, 797 (1938).
[30]R. Arians, T. Kümmell, G. Bacher, A. Gust, C. Kruse, and D. Hommel, Appl. Phys. Lett. **90**, 101114 (2007).
[31]E. W. Bogaart, J. E. M. Haverkort, T. Mano, T. Van Lippen, R. Nötzel, and J. H. Wolter, Phys. Rev. B **72**, 195301 (2005).
[32]T. Kümmell, R. Weigand, G. Bacher, A. Forchel, K. Leonardi, D. Hommel, and H. Selke, Appl. Phys. Lett. **73**, 3105 (1998).
[33]W.-M. Schulz, R. Roßbach, M. Reischle, G. J. Beirne, M. Bommer, M. Jetter, and P. Michler, Phys. Rev. B **79**, 035329 (2009).
[34]P. Dawson, O. Rubel, S. D. Baranovskii, K. Pierz, P. Thomas, and E. O. Göbel, Phys. Rev. B **72**, 235301 (2005).
[35]G. Bacher, C. Hartmann, H. Schweizer, T. Held, G. Mahler, and H. Nickel, Phys. Rev. B **47**, 9545 (1993).
[36]X. L. Zhou, Y. H. Chen, J. Q. Liu, B. Xu, X. L. Ye, and Z. G. Wang, Physica E **42**, 2455 (2010).
[37]P. Podemski, R. Kudraweic, J. Misiewicz, A. Somers, R. Schwertberger, J. P. Reithmaier, and A. Forchel, Appl. Phys. Lett. **89**, 151902 (2006).
[38]Y. Tang, D. H. Rich, I. Mukhametzhanov, P. Chen, and A. Madhukar, J. Appl. Phys. **84**, 3342 (1998).
[39]S. Khatsevich, D. H. Rich, E.-T. Kim, and A. Madhukar, J. Appl. Phys. **97**, 123520 (2005).
[40]W. D. Yang, R. R. Lowe-Webb, H. Lee, and P. C. Sercel, Phys. Rev. B **56**, 13314 (1997).
[41]M. Reischle, G. J. Beirne, W.-M. Schulz, M. Eichfelder, R. Roßbach, M. Jetter, and P. Michler, Opt. Exp. **16**(17), 12771–12776 (2008).
[42]A. K. Nowak, E. Gallardo, D. Sarkar, D. Sanvitto, H. P. van der Meulen, J. M. Calleja, J. M. Ripalda, L. González, and Y. González, Physica E **42**, 2509 (2010).
[43]K. Akahane, N. Ohtani, Y. Okada, and M. Kawabe, J. Crystal Growth **245**, 31 (2002).
[44]K. Akahane, N. Yamamoto, N. Ohtani, Y. Okada, and M. Kawabe, J. Crystal Growth **256**, 7 (2003).
[45]K. Akahane, N. Yamamoto, and T. Kawanishi, Phys. Status Solidi A **208**, 425 (2011).
[46]G. Balakrishnan, S. Huang, T. J. Rotter, A. Stintz, L. R. Dawson, K. J. Malloy, H. Xu, and D. L. Huffaker, Appl. Phys. Lett. **84**, 2058 (2004).
[47]M. A. Herman and H. Sitter, *Molecular Beam Epitaxy* (Springer, Berlin, 1989).
[48]J. Brault, M. Gendry, G. Grenet, G. Hollinger, Y. Desières, and T. Benyattou, Appl. Phys. Lett. **73**, 2932 (1998).
[49]S. Hinooda, S. Fréchengues, B. Lambert, S. Loualiche, M. Paillard, X. Marie, and T. Amand, Appl. Phys. Lett. **75**, 3530 (1999).
[50]Z. L. Yuan, E. R. A. D. Foo, J. F. Fyan, D. J. Mowbray, M. S. Skolnick, and M. Hopkinson, Phys. Status Solidi A **178**, 345 (2000).
[51]G. Gelinas, A. Lanacer, R. Leonnelli, R. A. Masut, and P. J.Poole, Phys. Rev. B **81**, 235426 (2010).
[52]E. C. Le Ru, J. Fack, and R. Murray, Phys. Rev. B **67**, 245318 (2003).
[53]P. Michler, A. Hangleiter, M. Moser, M. Geiger, and F. Scholz, Phys. Rev. B **46**, 7280 (1992).
[54]P. Ester, L. Lackmann, Vasconcellos S. Michaelis de, M. C. Hübner, A. Zrenner, and M. Bichler, Appl. Phys. Lett. **91**, 111110 (2007).
[55]W.-H. Chang, H. Lin, S.-Y. Wang, C.-H. Lin, S.-J. Cheng, and M.-C. Lee, Phys. Rev. B **77**, 245314 (2008).
[56]C. Hermannstädter, G. J. Beirne, M. Witzany, M. Heldmaier, J. Peng, G. Bester, L. Wang, A. Rastelli, O. G. Schmidt, and P. Michler, Phys. Rev. B **82**, 085309 (2010).
[57]I. Vurgaftman, J. R. Meyer, and L. R. Ram-Mohan, J. Appl. Phys. **89**, 5815 (2001).
[58]P. Borri, W. Langbein, U. Woggon, V. Stavarache, D. Reuter, and A. D. Wieck, Phys. Rev. B **71**, 115328 (2005).
[59]G. Rainò, G. Visimberga, A. Salhi, M. De Vittorio, and A. Passaseo, Appl. Phys. Lett. **90**, 111907 (2007).
[60]A. Patanè, A. Polimeni, M. Henini, L. Eaves, P. C. Main, and G. Hill, J. Appl. Phys. **85**, 625 (1999).
[61]X. Mu, Y. J. Ding, B. S. Ooi, and M. Hopkinson, Appl. Phys. Lett. **89**, 181924 (2006).
[62]A. Melliti, M. A. Maaref, F. Hassen, M. Hijiri, H. Maaref, J. Tignon, and B. Sermage, Solid State Commun. **128**, 213 (2003).
[63]G. Rainò, A. Salhi, V. Tasco, R. Intartagila, R. Congolani, Y. Rouillard, E. Tournié, and M. DeGiorgi, Appl. Phys. Lett. **92**, 101931 (2008).
[64]T. S. Shamirzaev, D. S. Abramkin, A. V. Nenashev, K. S. Zhuravlev, F. Trojánek, B. Dzurňák, and P. Malý, Nanotechnology **21**, 155703 (2010).
[65]K. Takemoto, Y. Sakuma, S. Hirose, T. Usuki, N. Yokoyama, T. Miyazawa, M. Takatsu, and Y. Arakawa, Physica E **26**, 185 (2005).
[66]J.-H. Huh, C. Hermannstädter, K. Akahane, H. Sasakura, N. A. Jahan, M. Sasaki, and I. Suemune, Jpn. J. Appl. Phys. Part 1 **50**, 06GG02 (2011).